remote sensing

MDPI

Article

Object-Based Change Detection in the Cerrado Biome Using Landsat Time Series

Inacio T. Bueno [1,*], Fausto W. Acerbi Júnior [1], Eduarda M. O. Silveira [1], José M. Mello [1], Luís M. T. Carvalho [1], Lucas R. Gomide [1], Kieran Withey [2] and José Roberto S. Scolforo [1]

[1] Forest Science Department, Federal University of Lavras, Lavras 37200-000, Brazil; fausto@dcf.ufla.br (F.W.A.J.); dudalavras@hotmail.com (E.M.O.S.); josemarcio@dcf.ufla.br (J.M.M.); passarinho@dcf.ufla.br (L.M.T.C.); lucasgomide@dcf.ufla.br (L.R.G.); jscolforo@dcf.ufla.br (J.R.S.S.)

[2] Lancaster Environment Centre, Lancaster University, Lancaster LA1 4YQ, UK; kieranwithey@gmail.com

* Correspondence: inaciotbueno@gmail.com; Tel.: +55-35-3822-1700

Received: 21 January 2019; Accepted: 4 March 2019; Published: 8 March 2019

check for updates

Abstract: Change detection methods are often incapable of accurately detecting changes within time series that are heavily influenced by seasonal variations. Techniques for de-seasoning time series or methods that apply the spatial context have been used to improve the results of change detection. However, few studies have explored Landsat's shortwave infrared channel (SWIR 2) to discriminate between seasonal changes and land use/land cover changes (LULCC). Here, we explored the effectiveness of Operational Land Imager (OLI) spectral bands and vegetation indices for detecting deforestation in highly seasonal areas of Brazilian savannas. We adopted object-based image analysis (OBIA), applying a multidate segmentation to an OLI time series to generate input data for discrimination of deforestation from seasonal changes using the Random Forest (RF) algorithm. We found adequate separability between deforested objects and seasonal changes using SWIR 2. Using spectral indices computed from SWIR 2, the RF algorithm generated a change map with an overall accuracy of 88.3%. For deforestation, the producer's accuracy was 88.0% and the user's accuracy was 84.6%. The SWIR 2 channel as well as the mid-infrared burn index presented the highest importance among spectral variables computed by the RF average impurity decrease measure. Our results give support to further change detection studies regarding to suitable spectral channels and provided a useful foundation for savanna change detection using an object-based method applied to Landsat time series.

Keywords: deforestation; savanna; vegetation seasonality; multidate segmentation; shortwave infrared

1. Introduction

The Cerrado (Brazilian savanna), is the second-largest biome in the country, covering approximately 2 million square kilometers, and exhibits the richest flora among savannas worldwide [1–3]. However, this biome has been subjected to rapid land cover conversion due to agriculture expansion, wood extraction, and relatively little of its area being protected by law [4]. In addition, the Cerrado is one of the least-studied biomes in the world [5,6] and has received little attention when compared to other Brazilian biomes like the Amazon and the Atlantic Forest, especially with respect to mapping and monitoring. Consequently, the understanding of land use and land cover change (LULCC) in this biome is limited.

Techniques and algorithms for mapping and monitoring the Cerrado have previously been developed by the scientific community [7], but the highly seasonal nature of this biome hampers LULCC detection [8]. When images from different seasons are acquired, changes caused by phenological differences are inevitable and pose a significant challenge to remotely sensed change detection [9]. The methods developed so far are often incapable of detecting changes within time series that are heavily influenced by seasonal climatic variations [10,11].

Object-based image analysis (OBIA) has become a common practice for LULCC detection, since it combines segmentation and remote sensing information along with the experience of the analyst to detect land cover change [12,13]. The use of OBIA increased following the Landsat Global Archive Consolidation (LGAC) initiative and the opening of their imagery archives in 2008, when millions of images became available, enabling time series studies throughout the world [14]. This has enabled gains in resolution and accuracy, and has also leveraged the development of governmental programs based on remotely sensed time series [15].

To reduce the seasonal variations captured by multi-temporal images, techniques for de-seasoning time series have been used based on the assumption that seasonal patterns can be identified and removed [10,16]. However, this assumption may not always hold true if the images in the time series are not acquired at regular intervals or there are gaps due to the presence of clouds [17]. To minimize the impacts of seasonality, methods combining images taken by different satellites [18,19] and that use the spatial context [17,20,21] have been developed. However, only a few studies have explored the ability of the second shortwave infrared channel (SWIR 2) from time series of Landsat imagery to accurately detect deforestation in highly seasonal ecosystems.

A shortwave infrared channel is present in many land monitoring optical sensors, such as the Operational Land Imager (OLI), which has the SWIR 1 and SWIR 2 (1560–1660 nm and 2100–2300 nm, respectively) channels [22]. In vegetation studies, these channels have shown lower reflectance than other spectral regions due to absorption caused by water and biochemical content of vegetation [23], which has motivated their use in the dry-season [24,25] and in wetland vegetation [26]. Although some studies have proposed using the shortwave infrared channel from Moderate Resolution Imaging Spectroradiometer (MODIS) to map forest cover loss [27] and a ratio-based computation to monitor forest damage [28], the SWIR 2 channel from the Landsat series has been rarely used in Cerrado change detection. Studies have recently assessed land cover changes [29–33], but the analysis and quantification of deforestation is still a challenge using spectral information [34]. Thus, change detection in the Cerrado biome is motivated by the previous assumptions, where an effective spectral analysis of the change matter is required to support change detection studies.

In this study, we explore the effectiveness of OLI spectral bands and vegetation indices for detecting deforestation in highly seasonal areas of the Cerrado biome, motivated by the following research questions: (a) is it possible to detect land cover change in areas affected by seasonality with high degrees of accuracy? (b) what spectral bands or vegetation indices can best discriminate Cerrado deforestation from phenological effects?

We used Landsat OLI time series from 2013 to 2014 to derive change objects through multi-temporal object change analysis and to assess spectral channels and indices to accurately detect LULCC in an area of Cerrado. We applied the Random Forest ensemble algorithm to discriminate deforestation events from those associated with phenological changes, which is a common misclassification problem in the Cerrado biome.

2. Materials and Methods

2.1. Study Area and Data

The study area is located in the Bacia Hidrográfica dos Afluentes Mineiros do Médio São Francisco (SF9), a watershed in northern Minas Gerais, Brazil (Figure 1a), where 59% of the area is covered by native vegetation with a wide range of types or physiognomies [35]. Cerrado formations cover 37% of the study area and are characterized by a unique vertically structured mosaic of plant formations [1,36,37] with sparse and short twisted trees, woodland areas that are represented by forest formations with dense canopy cover (known as Cerradão), riparian forests, wetlands with palm tree formations or Veredas, and grasslands [6]. The climate is described as tropical savanna (Aw) with a distinct dry winter and wet summer [38]. Approximately 90% of the rainfall is concentrated between October and April, with annual precipitation ranging from 1200 to 1800 mm. The dry season is quite distinct, with monthly precipitation as low as 0 mm. This strong seasonality results in a wide range of adaptive phenological strategies, such as leaf shedding in Cerrado trees, thus influencing the vegetation's spatial and spectral dynamics [39].

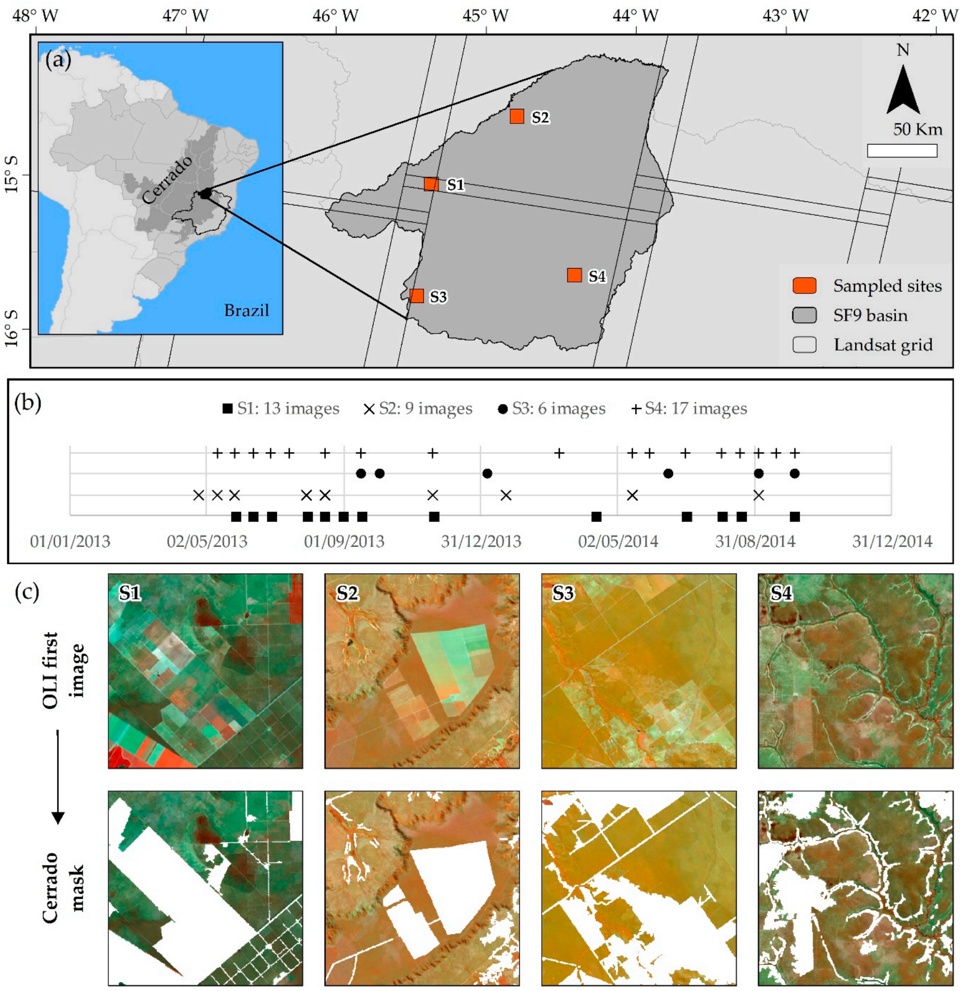

Figure 1. (**a**) The study area in the north of Minas Gerais (MG) state, Brazil, and the details of the sampling design; (**b**) cloud-free image acquisition dates per sampled site; (**c**) sampled areas represented by Landsat OLI image false color composition (Red = NIR, Green = SWIR 1, Blue = Red) and Cerrado mask layer from land cover classification.

We acquired cloud-free Landsat OLI images (path 219, rows 70 and 71) between April 2013 and December 2014 from the United States Geological Survey for Earth Observation and Science (USGS/EROS). The Landsat products were processed at Level-2, supporting time series analyses and data stacking with high precision [14] and bottom of atmosphere reflectance calculated [40]. We set a short two-year period because: (i) we can acquire and process images with lower time gaps and lower computational effort compared to long time series; (ii) the method can detect change events that may not be captured by a biannual method due to a rapid land conversion, for instance; (iii) a short period can generate annual deforestation reports, providing support for continuous monitoring and conservation applications.

Four sampling areas (10×10 km) that were covered by native vegetation and had undergone deforestation were selected by visual interpretation of Landsat imagery (Figure 1a). We defined deforestation (Def) as human-induced activities that completely remove the native vegetation, e.g., the conversion of native vegetation to pastures or bare soil by logging practices. Seasonal changes (Sch) were defined as stable native vegetation with no land cover conversion. Thus, two prerequisites were determined for image selection: absence of clouds and presence of deforested areas and seasonal changes, which led to different deforestation rates and image frequencies for each sampled site.

We generated a Cerrado mask based on a land cover classification using an object-based image analysis (OBIA) (Figure 1c). In this study, we applied the multi-resolution segmentation algorithm [41] implemented in the eCognition software (Munich, Germany) [42], to create image objects and classified them through Fuzzy logic and spectral parameter selections. Classification post-processing, such as visual interpretation and manual editing, corrected misclassifications improving the final map accuracy.

2.2. Change Detection

Our change detection method is divided into four main steps (Figure 2): (1) multidate segmentation, (2) feature extraction, (3) feature selection, (4) Random Forest classification.

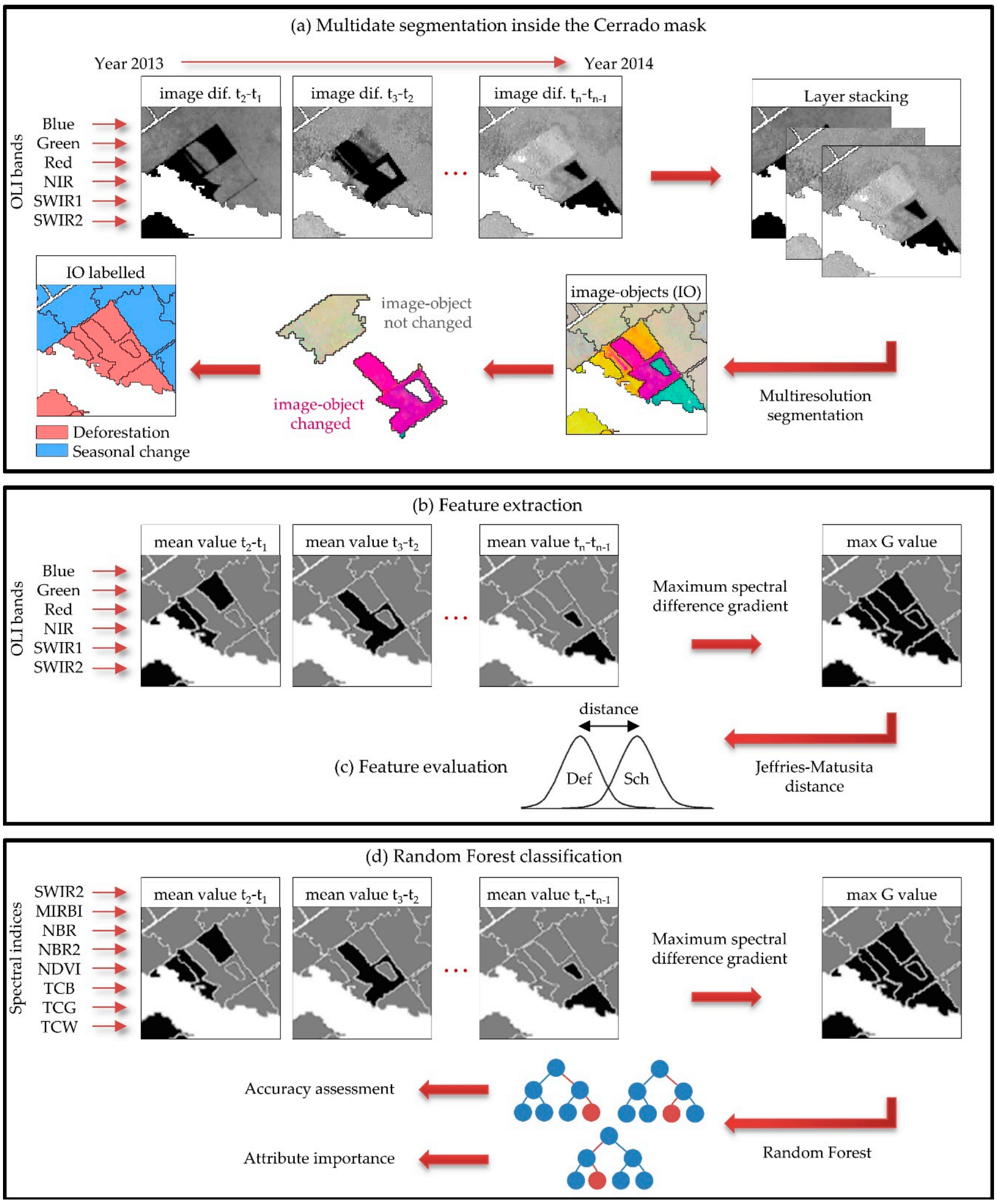

Figure 2. Schematic illustrating the change detection method. (**a**) Segmentation of multitemporal image objects; (**b**) Extraction of the maximum spectral difference gradient value; (**c**) Evaluation of OLI bands to separate deforestation from seasonal changes; (**d**) Random Forest classification of the image objects.

2.2.1. Multidate Segmentation

We created multitemporal image objects by segmenting multiple images difference of sequential periods. The procedure was conducted in a single operation using the whole set of spectral bands with sequential difference images together, which the layer stack dimension for each sampled site was determined by n − 1 (site image frequency) multiplied by six (OLI bands) [43]. This method incorporates spectral, spatial, and temporal information of difference images, which creates objects based on the feature dynamics in time such as change events in a vegetation background.

We applied the multi-resolution segmentation algorithm [41] using a trial-and-error approach [20,44] to find the appropriate segmentation parameters within the eCognition software. In this procedure, three parameters (shape, compactness, and scale) are used to guide the segmentation of image objects. We ran tests for the scale parameter at a rate of 1 to 100 with an interval of 25, and for compactness and shape a rate of 0.1 to 0.9 with intervals of 0.2. We set the shape to 0.1, the compactness to 0.5, and the scale to 50. The multidate segmentation output was evaluated based on visual assessment of segmentation suitability, where the scale parameter influenced directly the size of the objects by generating small and spurious information with low parameter values or merged multiple changed regions with high parameter values; compactness controlled the boundary of segments by generating smooth boundaries with low parameter values or compact with high values; and shape controlled the influence of spectral information on the formation of segments by creating color-influenced objects based on low parameter values or shape-influenced objects based on high values. Once the multidate segmentation was carried out, we labeled all image objects as Def or Sch by visual interpretation of the time series.

2.2.2. Feature Extraction

To extract information from the image objects, we calculated the mean pixel value inside the objects for all OLI spectral bands. Hence, the maximum spectral gradient difference (SGD) [9,45], was calculated based on the objects' means (i), where the higher positive value of $g_{(i,\,t,\,t-1)}$ in a band b, the larger spectral change from time index $t-1$ to t (Equation (1)).

$$g_{(i,b)\max} = \left[b_{(i,t)} - b_{(i,t-1)}\right]_{\max} \quad (1)$$

In general, objects labeled as deforestation (Figure 3a) presented higher g values than seasonal change objects (Figure 3b), as logging activity abruptly increases object reflectance and g value.

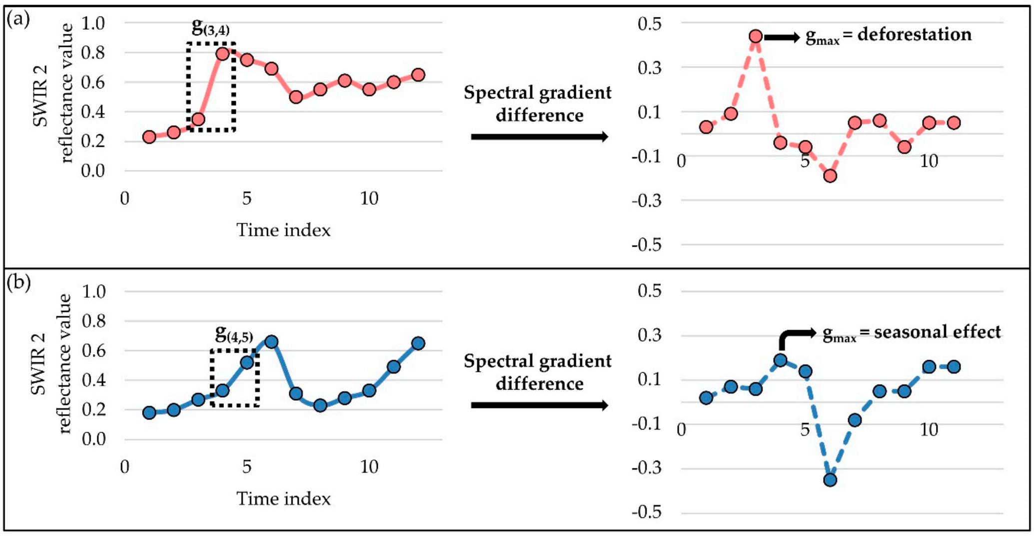

Figure 3. (**a**) Reflectance values, spectral gradient differences, and maximum g value of a Def object; and (**b**) of a Sch object.

2.2.3. Feature Evaluation

We first evaluated OLI bands to determine the ability of each band to separate deforestation from seasonal changes. Objects were initially classified as Def and Sch by a skilled interpreter, and then we sampled 100 objects per class (Def and Sch, 200 total) from the four study sites. We derived normalized sensor-specific Def and Sch distributions fitted by a Gaussian model to evaluated the Def/Sch separability for Landsat OLI bands using the normalized Jeffries-Matusita distance (JM), which has a finite dynamic range between 0 (totally inseparable) and 2 (totally separable) [46]. JM evaluation was performed in R statistical software (Vienna, Austria) using the varSel package [47].

Second, we selected a set of spectral indices derived from Landsat images to detect changed objects based on the SWIR 2 spectral channel (Table 1). Despite a large list of indices in the scientific literature, we selected band computations that span the spectrum of SWIR 2 and are sensitive to vegetation characteristics, conditions or changes. In addition, we computed tasseled cap transformations since the formula uses all OLI channels [48]. The NDVI was also maintained because it is the most frequently used spectral index in remote sensing science [49]. Once the spectral indices were computed, the maximum spectral gradient difference was also calculated for each of them and for the SWIR 2 band.

Table 1. Set of spectral variables evaluated for change detection.

Name	Abbreviation	Equation	Reference
Shortwave infrared spectral channel	SWIR 2	-	[22]
Mid Infrared Burned Index	MIRBI	$10 \times \text{SWIR2} + 9.8 \times \text{SWIR1} + 2$	[50]
Normalized Burn Ratio	NBR	$\frac{\text{NIR} - \text{SWIR2}}{\text{NIR} + \text{SWIR2}}$	[51]
Normalized Burn Ratio 2	NBR 2	$\frac{\text{SWIR1} - \text{SWIR2}}{\text{SWIR1} + \text{SWIR2}}$	[15]
Normalized Difference Vegetation Index	NDVI	$\frac{\text{NIR} - \text{R}}{\text{NIR} + \text{R}}$	[52]
Tasseled Cap Brightness	TCB	$b_1 \times B + b_2 \times G + b_3 \times R + b_4 \times \text{NIR} + b_5 \times \text{SWIR1} + b_6 \times \text{SWIR2}$	[48]
Tasseled Cap Greenness	TCG	$g_1 \times B + g_2 \times G + g_3 \times R + g_4 \times \text{NIR} + g_5 \times \text{SWIR1} + g_6 \times \text{SWIR2}$	[48]
Tasseled Cap Wetness	TCW	$w_1 \times B + w_2 \times G + w_3 \times R + w_4 \times \text{NIR} + w_5 \times \text{SWIR1} + w_6 \times \text{SWIR2}$	[48]

2.2.4. Random Forest Classification

Random forest (RF) [53] has been increasingly applied in remote sensing studies [54], because it offers key advantages over other methods, such as its non-parametric nature, higher classification accuracy, and capability to determine variable importance [55]. First, we split the 200 SGD values derived from image objects into two datasets: 140 observations for training (70% of the sample) and 60 for the test set (the remaining 30%). The training set was used to fit the RF model while the test set was used to assess the generalization error of the best fitted model. Although the test set contains the pre-classified results, it ran against the fitted model and the model results were compared to the unused pre-classified data and then evaluated by a confusion matrix. RF requires two user-defined parameters to be set: the number of decision trees (Ntree) and the number of attributes to be tested for the best split (Mtry). We set Ntree to 500 and Mtry to 3 (square root of the number of input variables) according to previous remote sensing studies [54].

Overall accuracy, user's accuracy (inversely related to commission error), and producer's accuracy (inversely related to omission error), were used to assess the accuracy of the trained RF classifier applied to the test set [56]. In addition, accuracy metrics were also performed by each site separately.

We computed the importance of spectral variables by analyzing the average impurity decrease. RF switches one of the input random variables while keeping the rest constant and measures the decrease in impurity by means of the Gini index. The difference between the general average and the variable evaluation average were used to rank the importance of each spectral variable in the change detection procedure, where the higher the difference, the higher the importance of a particular variable [55].

3. Results

3.1. Feature Evaluation

The Def and Sch distributions overlaid with the respective probability density functions fitted separately for each Landsat OLI band are illustrated in Figure 4. According to the JM distance, the SWIR 2 band presented the strongest Def/Sch separability among the OLI bands (JM = 0.92). Bands in the visible spectrum also presented reasonable separability, and NIR presented the weakest measure (JM = 0.17).

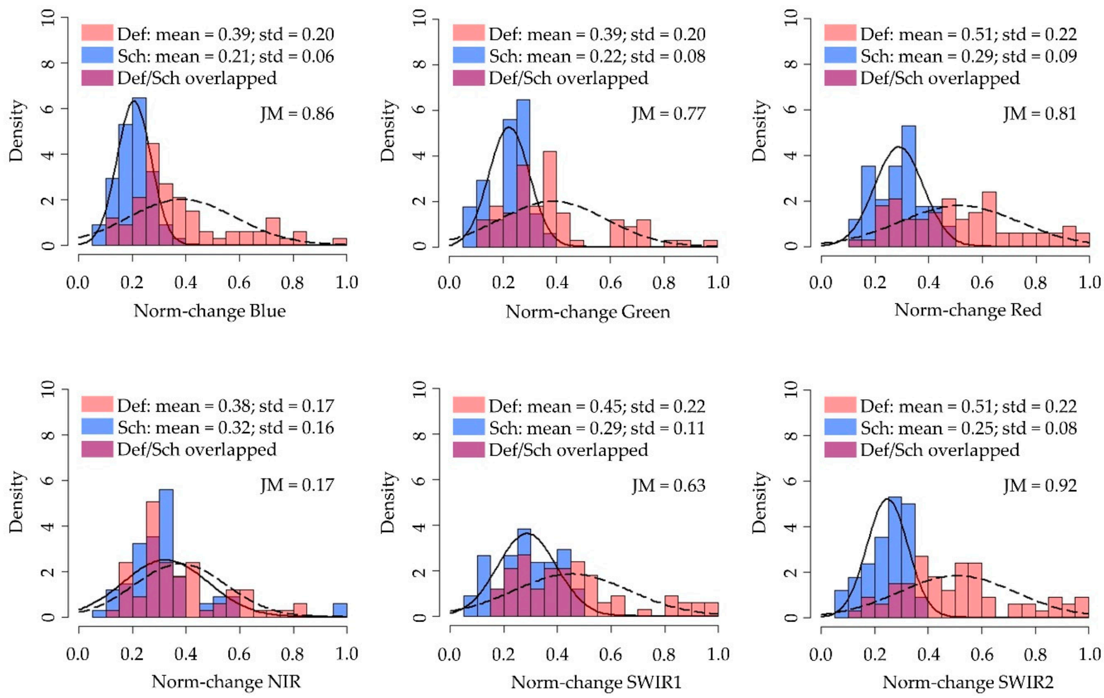

Figure 4. Deforestation (Def) and seasonal change (Sch) distributions overlaid with probability density function (pdf) fitted separately for each Landsat OLI band mean and standard deviation (std) of the derived pdfs and the Jeffries-Matusita (JM) distance are given. JM ranges between 0 (total inseparable) to 2 (total separable).

3.2. Change Detection

The Random Forest (RF) algorithm constructed 500 trees using spectral indices based on SWIR 2, NDVI, Tasseled cap transformations, and the SWIR 2 surface reflectance data. The RF classified the test set with overall accuracy of 88.3%. The producer's accuracy was 88.0% (omission error of 12.0%) and the user's accuracy was 84.6% (commission error of 15.4%) for the Def class (Table 2). The overall accuracy by site demonstrated low variability among all sites, with Site 3 presenting the highest value (93.3%) and Site 1 the lowest value (83.3%). The Def class presented good producer and user's accuracies, except the user's accuracy of 57.1% in site 2. Accuracies for the change maps of the sampled sites are shown in Figure 5.

Table 2. Accuracy analysis results from change detection, represented by overall accuracy and its complementary measure, overall error; producer's accuracy and its complementary measure omission error (O.E.); and user's accuracy and its complementary measure commission error (C.E.).

Site	Overall Accuracy (%)	Overall Error (%)	Producer's Accuracy (%)				User's Accuracy (%)			
			Def	O.E.	Sch	O.E.	Def	C.E.	Sch	C.E.
All	88.3	11.7	88.0	12.0	88.6	11.4	84.6	15.4	91.2	8.8
1	83.3	11.7	75.0	25.0	100.0	0.0	100.0	0.0	67.7	32.3
2	87.5	12.5	100.0	0.0	75.0	25.0	57.1	42.9	100.0	0.0
3	93.3	6.7	100.0	0.0	87.5	12.5	87.6	12.4	100.0	0.0
4	86.7	13.3	80.0	20.0	90.0	10.0	80.0	20.0	90.0	10.0

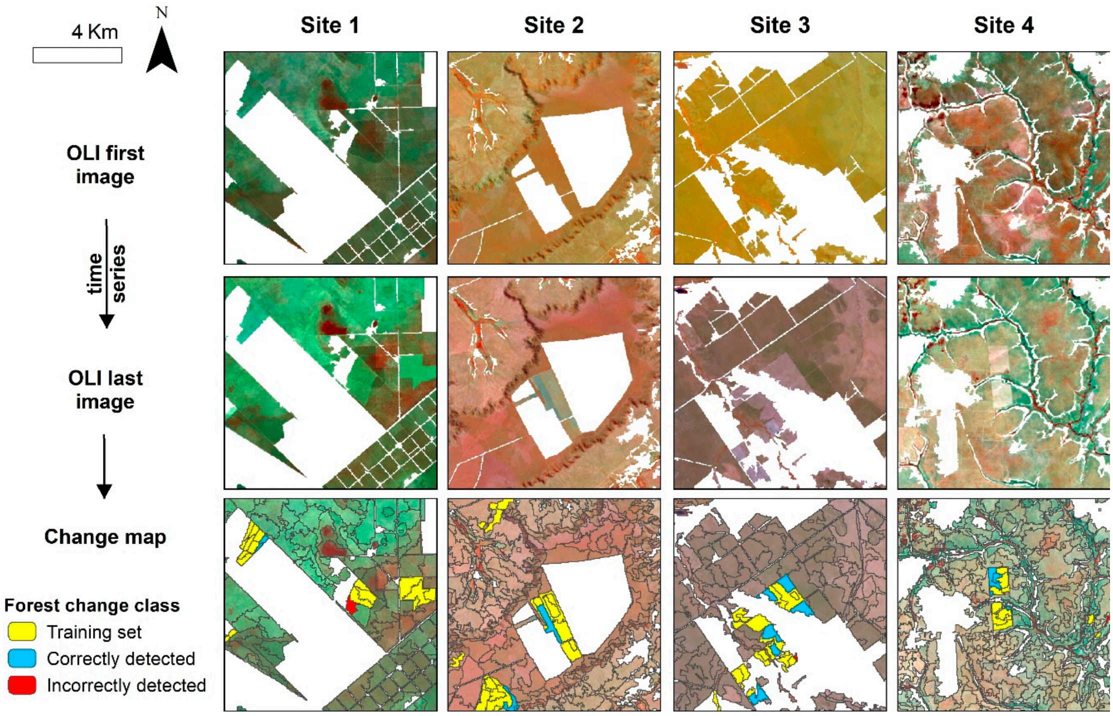

Figure 5. Change maps for the 2013–2014 period.

The importance of each spectral variable related to average impurity decrease is shown in Figure 6. The SWIR 2 and the MIRBI index emerged as the most important spectral variables in the Random Forest classification. Tasseled cap and NDVI performed poorly among the other spectral variables.

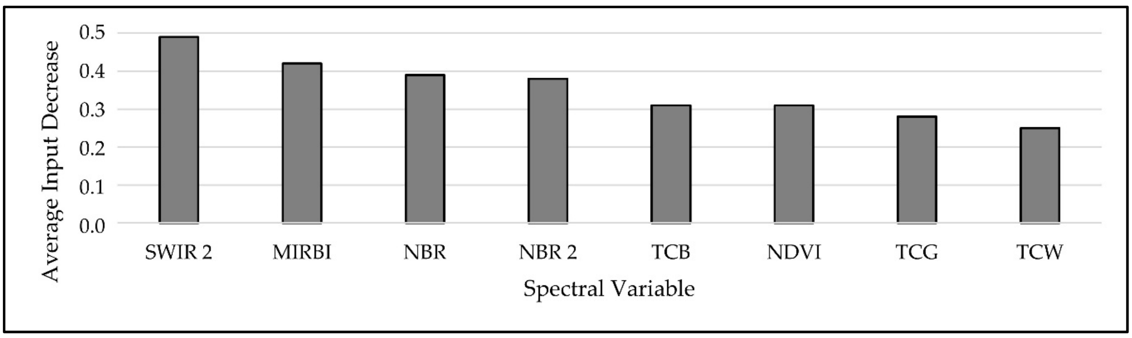

Figure 6. Importance of spectral variables in the Random Forest change detection.

4. Discussion

4.1. Emerging Options for Change Detection in the Cerrado

Despite the NDVI being the most frequently used index in remote sensing science [49], we have demonstrated that the SWIR 2 band is useful for land cover change detection because it is affected to a lesser extent by atmospheric noise and generally has low values for forests but high values for soil and non-photosynthetic components of vegetation (e.g., bark, branches, and dry leaves) [57]. Based on the reflectance values of near infrared and red channels in forests and bare soils objects [58], NDVI is very sensitive to variations in extant vegetation, but may not be relevant where these applications are related to other land cover classes, e.g., conversion of vegetation into bare soil.

Here, we have shown that SWIR 2 is a suitable channel to discriminate deforestation events, even when faced with high levels of seasonal noise and a large amount of non-photosynthetic material. The importance and utility of SWIR wavelengths (single band and derived indices) for characterizing forest structure have also been highlighted in several other applications, such as disturbance detection over forested systems [49,59], mapping forest loss [27] and damage [28], analysis of post-fire conditions [60], and forest recovery [61]. SWIR has also been advocated for characterizing [1] and detecting burn events [62–65] in Cerrado regions.

Although SWIR 2 has the potential to be used to detect deforestation, the Def and Sch distributions for this band resulted in a Jeffries-Matusita separability of 0.92 (scale of 0–2), meaning misclassifications between deforestation and seasonal changes were common. Studies have pointed out the limitation of this measure due to the strong seasonality in NDVI forested and non-forested distributions suggesting a spatial normalization to improve JM separability [46].

A new option to detect changes in Cerrado and perhaps in seasonal savannas in general emerges building upon a better understanding of the complete change event. To accurately detect land conversions, the post-change land cover class must be also understood, such as their reflectance values, and the spectral differences to the pre-change class. For instance, if a forested area is converted to bare soil or a water body, SWIR 2 using the methodology presented here would be suitable for this type of change detection, but if the same area is quickly converted to a crop field or initial forest regeneration, another spectral channel may be more suitable.

4.2. Detecting and Quantifying Deforestation through Time

Our second research question was concerned with distinguishing deforestation from seasonal changes. Our approach to deforestation detection using RF and a dataset derived from SWIR 2 temporal metrics performed well, with the RF being robust and easy to implement while producing accurate results based on the maximum spectral gradient difference.

Producer's and user's accuracies presented similar prediction errors for all sites. The commission error of Sch (15.4%) indicates a low inclusion of areas affected by seasonal noise in the deforestation class, which remains a considerable challenge for change detection studies in seasonal environments. We believe several aspects of our approach contributed to these high levels of accuracy: (i) the maximum spectral gradient difference parameter used for discriminating deforestation from seasonal change; (ii) the use of cloud-free imagery and constant sample interval in the temporal domain for each study site; (iii) the use of a Cerrado mask generated by land cover classification allowing an accurate input dataset for change detection; and (iv) the visual assessment of multidate segmentation, suggesting that deforestation events were effectively represented by the image objects, even when affected by seasonal noise.

The overall accuracy analysis for each site demonstrated low variability (83.3 to 93.3%), while producer' and user's accuracies presented fluctuating measures for the Def class (75 to 100% and 57.1 to 100%, respectively). However, these accuracies per site are likely unreliable since the test set was randomly sampled from the four sites, thus the change object frequency is most likely different for each site and may not be enough for a reliable site-specific accuracy analysis. In other words, the image frequency can affect the number of deforested areas detected per site, which in turn, will affect the accuracy results. For instance, an omission error of one changed object in a site where only two changed objects were detected means an error of 50%, whereas in a site where five changed objects were detected an omission error of one changed object means an error of 20%.

The importance of each spectral channel related to average impurity also ranked SWIR 2 as the most important spectral variable in the RF change detection, followed by MIRBI and NBR. The performance of SWIR 2 must be emphasized not only for its ability to discriminate deforestation, but also for its greater separability using the Jeffries-Matusita distance between fitted distributions. Furthermore, the low importance of NDVI in the change detection and the separability of the near infrared channel being the lowest are noteworthy. Tasseled cap transformations were also poor inputs to the RF change detection. This may be explained by a weak coefficient relationship with our study area since tasseled cap coefficients were not fitted in the Cerrado [48].

4.3. Method Limitations

Some limitations to this method are apparent, such as sampling considerations, timing of changes, application to large datasets, and deforestation occurrence.

We sampled the study area to reduce computational and operational efforts, and to understand the data better. Heterogeneous landscapes in terms of vegetation gradients must be stratified to reduce mixed information since large areas can lead to uncertainties in change detection.

The timing of change is important to forest monitoring. Although the temporal information was available during the multidate segmentation procedure, the timings of change events were not tracked. This is a crucial limitation in terms of the method's continuity and consistency, which reduces its applicability in monitoring studies/programs.

The use of a large number of images in a time series can be an issue in terms of storage space and computational time, but as discussed in this study, large sets can be reduced since small differences in the number of images may not affect the detection of changed areas. Nevertheless, the higher the number of images in the time series, the larger the amount of temporal and spectral information in the segmentation process. Large amounts of temporal (long time series), spectral (multiple bands) and spatial information (large areas) might hamper multidate segmentation by prohibitively increasing processing time and by creating small and spurious objects. Even though the computational time in this study took less than a minute for each site to be processed by one computer, it is important to consider the sample size of 100 km^2 per site, which represents 0.2% of Minas Gerais state, and large areas as would take hours of processing time.

In particular situations, our method may not detect deforestation when it occurs in the last two images and the seasonal noise is still very strong. In this situation, Cerrado trees are mostly non-photosynthetic and the increase in reflectance caused by deforestation may be not be detected as forest change, because another observation must be included to detect the change. In that case, monitoring studies, which continuously acquire observations and imagery, can avoid these undetected change events. Thus, this limitation must be explored in the Cerrado, since the difficulty of change detection in this biome is widely recognized.

5. Conclusions

We have explored the spectral information extracted from Landsat OLI time series to accurately detect deforestation in Brazilian seasonal savannas. We have demonstrated that the Landsat OLI SWIR 2 band presented the highest change detection accuracy, differentiating deforestation from seasonal changes and resulting in fewer misclassifications.

The Random Forest algorithm presented satisfactory change detection accuracies and highlighted SWIR 2 and MIRBI as important spectral variables. Future studies may be able to use a subset of the most important spectral variables, such as SWIR 2 and MIRBI, to reduce the storage and computational demands for segmentation and change detection.

Future research should follow-up this approach by exploring different data sources such as Sentinel imagery, along with the use of different classifiers. Further studies should also improve upon the current method by addressing the issues discussed above, such as the sampling factor, timing of changes, particular change events, and the processing of large spatial (extensive areas) and/or temporal (long time series) datasets. In addition, the response of SWIR 2 to different target classes, such as non-native vegetation, should be investigated further.

Author Contributions: These authors equally contributed to this work.

Funding: This research received no external funding.

Acknowledgments: The authors are grateful to the Coordenação de Aperfeiçoamento de Pessoal de Nível Superior (CAPES), the Conselho Nacional de Desenvolvimento Científico e Tecnológico (CNPq), and the Fundação de Amparo à Pesquisa do Estado de Minas Gerais (FAPEMIG) for supporting this work.

Conflicts of Interest: The authors declare no conflicts of interest.

References

1. Hill, M.J.; Zhou, Q.; Sun, Q.; Schaaf, C.B.; Palace, M. Relationships between vegetation indices, fractional cover retrievals and the structure and composition of Brazilian Cerrado natural vegetation. *Int. J. Remote Sens.* **2017**, *38*, 874–905. [CrossRef]
2. Myers, N.; Mittermeier, R.A.; Mittermeier, C.G.; Fonseca, G.A.B.; Kent, J. Biodiversity hotspots for conservation priorities. *Nature* **2000**, *403*, 853–858. [CrossRef] [PubMed]
3. Klink, C.A.; Machado, R.B. Conservation of the Brazilian Cerrado. *Conserv. Biol.* **2005**, *19*, 707–713. [CrossRef]
4. MMA. *Monitoramento Do Desmatamento nos Biomas Brasileiros Por Satélite: Cerrado 2009–2010*; Ministério do Meio Ambiente: Brasília, Brazil, 2011.
5. Menino, G.C.O.; Nunes, Y.R.F.; Santos, R.M.; Fernandes, G.W.; Fernandes, L.A. Environmental heterogeneity and natural regeneration in riparian vegetation of the brazilian semi-arid region. *Edinb. J. Bot.* **2012**, *69*, 29–51. [CrossRef]
6. Ribeiro, J.F.; Walter, B.M.T. As principais fitofisionomias do bioma Cerrado. In *Cerrado: Ecologia e Flora*; Embrapa Cerrados/Embrapa Informação Tecnológica: Planaltina, Brazil, 2008; pp. 152–212, ISBN 978-85-7383-397-3.
7. Hussain, M.; Chen, D.; Cheng, A.; Wei, H.; Stanley, D. Change detection from remotely sensed images: From pixel-based to object-based approaches. *ISPRS J. Photogramm. Remote Sens.* **2013**, *80*, 91–106. [CrossRef]
8. Tewkesbury, A.P.; Comber, A.J.; Tate, N.J.; Lamb, A.; Fisher, P.F. A critical synthesis of remotely sensed optical image change detection techniques. *Remote Sens. Environ.* **2015**, *160*, 1–14. [CrossRef]
9. Lu, M.; Chen, J.; Tang, H.; Rao, Y.; Yang, P.; Wu, W. Land cover change detection by integrating object-based data blending model of Landsat and MODIS. *Remote Sens. Environ.* **2016**, *184*, 374–386. [CrossRef]
10. Verbesselt, J.; Hyndman, R.; Newnham, G.; Culvenor, D. Detecting trend and seasonal changes in satellite image time series. *Remote Sens. Environ.* **2010**, *114*, 106–115. [CrossRef]
11. Lu, D.; Mausel, P.; Brondízio, E.; Moran, E. Change detection techniques. *Int. J. Remote Sens.* **2004**, *25*, 2365–2407. [CrossRef]
12. Blaschke, T. Object based image analysis for remote sensing. *ISPRS J. Photogramm. Remote Sens.* **2010**, *65*, 2–16. [CrossRef]
13. Chen, G.; Hay, G.J.; Carvalho, L.M.T.; Wulder, M.A. Object-based change detection. *Int. J. Remote Sens.* **2012**, *33*, 4434–4457. [CrossRef]
14. Zhu, Z. Change detection using landsat time series: A review of frequencies, preprocessing, algorithms, and applications. *ISPRS J. Photogramm. Remote Sens.* **2017**, *130*, 370–384. [CrossRef]
15. DeVries, B.; Pratihast, A.K.; Verbesselt, J.; Kooistra, L.; Herold, M. Characterizing Forest Change Using Community-Based Monitoring Data and Landsat Time Series. *PLoS ONE* **2016**, *11*, e0147121. [CrossRef] [PubMed]
16. Verbesselt, J.; Hyndman, R.; Zeileis, A.; Culvenor, D. Phenological change detection while accounting for abrupt and gradual trends in satellite image time series. *Remote Sens. Environ.* **2010**, *114*, 2970–2980. [CrossRef]

17. Hamunyela, E.; Verbesselt, J.; Herold, M. Using spatial context to improve early detection of deforestation from Landsat time series. *Remote Sens. Environ.* **2016**, *172*, 126–138. [CrossRef]
18. Dutrieux, L.P.; Verbesselt, J.; Kooistra, L.; Herold, M. Monitoring forest cover loss using multiple data streams, a case study of a tropical dry forest in Bolivia. *ISPRS J. Photogramm. Remote Sens.* **2015**, *107*, 112–125. [CrossRef]
19. Zhang, J. Multi-source remote sensing data fusion: Status and trends. *Int. J. Image Data Fusion* **2010**, *1*, 5–24. [CrossRef]
20. Silveira, E.; Bueno, I.; Acerbi-Junior, F.; Mello, J.; Scolforo, J.; Wulder, M. Using Spatial Features to Reduce the Impact of Seasonality for Detecting Tropical Forest Changes from Landsat Time Series. *Remote Sens.* **2018**, *10*, 808. [CrossRef]
21. Silveira, E.M.D.O.; Mello, J.M.D.; Acerbi Júnior, F.W.; Carvalho, L.M.T.D. Object-based land-cover change detection applied to Brazilian seasonal savannahs using geostatistical features. *Int. J. Remote Sens.* **2018**, *39*, 2597–2619. [CrossRef]
22. Barsi, J.; Lee, K.; Kvaran, G.; Markham, B.; Pedelty, J. The Spectral Response of the Landsat-8 Operational Land Imager. *Remote Sens.* **2014**, *6*, 10232–10251. [CrossRef]
23. Ustin, S.L.; Roberts, D.A.; Gamon, J.A.; Asner, G.P.; Green, R.O. Using Imaging Spectroscopy to Study Ecosystem Processes and Properties. *Bioscience* **2004**, *54*, 523–534. [CrossRef]
24. Jacques, D.C.; Kergoat, L.; Hiernaux, P.; Mougin, E.; Defourny, P. Monitoring dry vegetation masses in semi-arid areas with MODIS SWIR bands. *Remote Sens. Environ.* **2014**, *153*, 40–49. [CrossRef]
25. Kergoat, L.; Hiernaux, P.; Dardel, C.; Pierre, C.; Guichard, F.; Kalilou, A. Dry-season vegetation mass and cover fraction from SWIR1.6 and SWIR2.1 band ratio: Ground-radiometer and MODIS data in the Sahel. *Int. J. Appl. Earth Obs. Geoinf.* **2015**, *39*, 56–64. [CrossRef]
26. Adam, E.; Mutanga, O.; Rugege, D. Multispectral and hyperspectral remote sensing for identification and mapping of wetland vegetation: A review. *Wetl. Ecol. Manag.* **2010**, *18*, 281–296. [CrossRef]
27. Potapov, P.; Hansen, M.C.; Stehman, S.V.; Loveland, T.R.; Pittman, K. Combining MODIS and Landsat imagery to estimate and map boreal forest cover loss. *Remote Sens. Environ.* **2008**, *112*, 3708–3719. [CrossRef]
28. Vogelmann, J.E.; Tolk, B.; Zhu, Z. Monitoring forest changes in the southwestern United States using multitemporal Landsat data. *Remote Sens. Environ.* **2009**, *113*, 1739–1748. [CrossRef]
29. Brannstrom, C.; Jepson, W.; Filippi, A.M.; Redo, D.; Xu, Z.; Ganesh, S. Land change in the Brazilian Savanna (Cerrado), 1986–2002: Comparative analysis and implications for land-use policy. *Land Use Policy* **2008**, *25*, 579–595. [CrossRef]
30. Coelho, V.H.R.; Montenegro, S.M.G.L.; Almeida, C.N.; Lima, E.R.V.; Ribeiro Neto, A.; Moura, G.S.S. Dinâmica do uso e ocupação do solo em uma bacia hidrográfica do semiárido brasileiro. *Rev. Bras. Eng. Agrícola e Ambient.* **2014**, *18*, 64–72. [CrossRef]
31. Beuchle, R.; Grecchi, R.C.; Shimabukuro, Y.E.; Seliger, R.; Eva, H.D.; Sano, E.; Achard, F. Land cover changes in the Brazilian Cerrado and Caatinga biomes from 1990 to 2010 based on a systematic remote sensing sampling approach. *Appl. Geogr.* **2015**, *58*, 116–127. [CrossRef]
32. Grecchi, R.C.; Gwyn, Q.H.J.; Bénié, G.B.; Formaggio, A.R.; Fahl, F.C. Land use and land cover changes in the Brazilian Cerrado: A multidisciplinary approach to assess the impacts of agricultural expansion. *Appl. Geogr.* **2014**, *55*, 300–312. [CrossRef]
33. Grecchi, R.C.; Gwyn, Q.H.J.; Bénié, G.B.; Formaggio, A.R. Assessing the spatio-temporal rates and patterns of land-use and land-cover changes in the Cerrados of southeastern Mato Grosso, Brazil. *Int. J. Remote Sens.* **2013**, *34*, 5369–5392. [CrossRef]
34. Trancoso, R.; Sano, E.E.; Meneses, P.R. The spectral changes of deforestation in the Brazilian tropical savanna. *Environ. Monit. Assess.* **2015**, *187*, 4145. [CrossRef] [PubMed]
35. Carvalho, L.M.T.; Scolforo, J.R.S. *Inventário Florestal de Minas Gerais: Monitoramento da Flora Nativa 2005–2007*; Editora UFLA: Lavras, Brazil, 2008; ISBN 978-85-87692-61-0.
36. Ratter, J.A.; Ribeiro, J.F.; Bridgewater, S. The Brazilian cerrado vegetation and threats to its biodiversity. *Ann. Bot.* **1997**, *80*, 223–230. [CrossRef]
37. Ferreira, L.; Yoshioka, H.; Huete, A.; Sano, E.E. Seasonal landscape and spectral vegetation index dynamics in the Brazilian Cerrado: An analysis within the Large-Scale Biosphere–Atmosphere Experiment in Amazônia (LBA). *Remote Sens. Environ.* **2003**, *87*, 534–550. [CrossRef]

38. Peel, M.C.; Finlayson, B.L.; McMahon, T.A. Updated world map of the Köppen-Geiger climate classification. *Hydrol. Earth Syst. Sci.* **2007**, *11*, 1633–1644. [CrossRef]
39. Ferreira, L.G.; Huete, A.R. Assessing the seasonal dynamics of the Brazilian Cerrado vegetation through the use of spectral vegetation indices. *Int. J. Remote Sens.* **2004**, *25*, 1837–1860. [CrossRef]
40. Vermote, E.F.; Justice, C.; Claverie, M.; Franch, B. Preliminary analysis of the performance of the Landsat 8/OLI land surface reflectance product. *Remote Sens. Environ.* **2016**, *185*, 46–56. [CrossRef]
41. Baatz, M.; Schäpe, A. Multiresolution segmentation: An optimization approach for high quality multi-scale image segmentation. In *Angewandte Geographische Informations-Verarbeitung, XII*; Wichmann Verlag: Karlsruhe, Germany, 2000; Volume 58, pp. 12–23.
42. Definiens, A. *Definiens eCognition Developer 8 User Guide*; Definies AG: Munich, Germany, 2009.
43. Desclée, B.; Bogaert, P.; Defourny, P. Forest change detection by statistical object-based method. *Remote Sens. Environ.* **2006**, *102*, 1–11. [CrossRef]
44. Duro, D.C.; Franklin, S.E.; Dubé, M.G. A comparison of pixel-based and object-based image analysis with selected machine learning algorithms for the classification of agricultural landscapes using SPOT-5 HRG imagery. *Remote Sens. Environ.* **2012**, *118*, 259–272. [CrossRef]
45. Chen, J.; Lu, M.; Chen, X.; Chen, J.; Chen, L. A spectral gradient difference based approach for land cover change detection. *ISPRS J. Photogramm. Remote Sens.* **2013**, *85*, 1–12. [CrossRef]
46. Reiche, J.; Hamunyela, E.; Verbesselt, J.; Hoekman, D.; Herold, M. Improving near-real time deforestation monitoring in tropical dry forests by combining dense Sentinel-1 time series with Landsat and ALOS-2 PALSAR-2. *Remote Sens. Environ.* **2018**, *204*, 147–161. [CrossRef]
47. Dalponte, M.; Orka, H.O.; Gobakken, T.; Gianelle, D.; Naesset, E. Tree Species Classification in Boreal Forests With Hyperspectral Data. *IEEE Trans. Geosci. Remote Sens.* **2013**, *51*, 2632–2645. [CrossRef]
48. Baig, M.H.A.; Zhang, L.; Shuai, T.; Tong, Q. Derivation of a tasselled cap transformation based on Landsat 8 at-satellite reflectance. *Remote Sens. Lett.* **2014**, *5*, 423–431. [CrossRef]
49. Schultz, M.; Clevers, J.G.P.W.; Carter, S.; Verbesselt, J.; Avitabile, V.; Quang, H.V.; Herold, M. Performance of vegetation indices from Landsat time series in deforestation monitoring. *Int. J. Appl. Earth Obs. Geoinf.* **2016**, *52*, 318–327. [CrossRef]
50. Trigg, S.; Flasse, S. An evaluation of different bi-spectral spaces for discriminating burned shrub-savannah. *Int. J. Remote Sens.* **2001**, *22*, 2641–2647. [CrossRef]
51. Key, C.H.; Benson, N.C. Landscape assessment: Ground measure of severity, the composite burn index; and remote sensing of severity, the normalized burn ratio. In *FIREMON: Fire Effects Monitoring and Inventory System. Gen. Tech. Rpt. RMRS-GTR-164-CD: LAI-15*; USDA Forest Service, Rocky Mountain Research Station: Ogden, UT, USA, 2006; p. 51, ISBN RMRS-GTR-164-CD.
52. Rouse, J.W.; Hass, R.H.; Schell, J.A.; Deering, D.W. Monitoring vegetation systems in the great plains with ERTS. In *Third Earth Resources Technology Satellite-1 Symposium*; NASA: Washington, DC, USA, 1973; Volume 1, pp. 309–317.
53. Breiman, L. Random Forests. *Mach. Learn.* **2001**, *45*, 5–32. [CrossRef]
54. Belgiu, M.; Drăguţ, L. Random forest in remote sensing: A review of applications and future directions. *ISPRS J. Photogramm. Remote Sens.* **2016**, *114*, 24–31. [CrossRef]
55. Rodriguez-Galiano, V.F.; Ghimire, B.; Rogan, J.; Chica-Olmo, M.; Rigol-Sanchez, J.P. An assessment of the effectiveness of a random forest classifier for land-cover classification. *ISPRS J. Photogramm. Remote Sens.* **2012**, *67*, 93–104. [CrossRef]
56. Congalton, R.G.; Green, K. *Assessing the Accuracy of Remotely Sensed Data: Principles and Practices*; CRC Press/Taylor & Francis: Boca Raton, FL, USA, 2009; ISBN 9781420055139.
57. Banskota, A.; Kayastha, N.; Falkowski, M.J.; Wulder, M.A.; Froese, R.E.; White, J.C. Forest Monitoring Using Landsat Time Series Data: A Review. *Can. J. Remote Sens.* **2014**, *40*, 362–384. [CrossRef]
58. Guerschman, J.P.; Hill, M.J.; Renzullo, L.J.; Barrett, D.J.; Marks, A.S.; Botha, E.J. Estimating fractional cover of photosynthetic vegetation, non-photosynthetic vegetation and bare soil in the Australian tropical savanna region upscaling the EO-1 Hyperion and MODIS sensors. *Remote Sens. Environ.* **2009**, *113*, 928–945. [CrossRef]
59. Cohen, W.B.; Yang, Z.; Healey, S.P.; Kennedy, R.E.; Gorelick, N. A LandTrendr multispectral ensemble for forest disturbance detection. *Remote Sens. Environ.* **2018**, *205*, 131–140. [CrossRef]

60. Wulder, M.A.; White, J.C.; Alvarez, F.; Han, T.; Rogan, J.; Hawkes, B. Characterizing boreal forest wildfire with multi-temporal Landsat and LIDAR data. *Remote Sens. Environ.* **2009**, *113*, 1540–1555. [CrossRef]
61. Cohen, W.B.; Yang, Z.; Kennedy, R. Detecting trends in forest disturbance and recovery using yearly Landsat time series: 2. TimeSync—Tools for calibration and validation. *Remote Sens. Environ.* **2010**, *114*, 2911–2924. [CrossRef]
62. Dacamara, C.C.; Libonati, R.; Ermida, S.L.; Calado, T.J. A User-Oriented Simplification of the (V,W) Burn-Sensitive Vegetation Index System. *IEEE Geosci. Remote Sens. Lett.* **2016**, *13*, 1822–1826. [CrossRef]
63. Libonati, R.; Dacamara, C.C.; Pereira, J.M.C.; Peres, L.F. On a new coordinate system for improved discrimination of vegetation and burned areas using MIR/NIR information. *Remote Sens. Environ.* **2011**, *115*, 1464–1477. [CrossRef]
64. Libonati, R.; Dacamara, C.C.; Pereira, J.M.C.; Peres, L.F. Retrieving middle-infrared reflectance using physical and empirical approaches: Implications for burned area monitoring. *IEEE Trans. Geosci. Remote Sens.* **2012**, *50*, 281–294. [CrossRef]
65. Pereira, A.A.; Pereira, J.M.C.; Libonati, R.; Oom, D.; Setzer, A.W.; Morelli, F.; Machado-Silva, F.; Carvalho, L.M.T. Burned area mapping in the Brazilian Savanna using a one-class support vector machine trained by active fires. *Remote Sens.* **2017**, *9*, 1161. [CrossRef]